

Shadow of rotating regular black holesAhmadjon Abdujabbarov,^{1,2,3,*} Muhammed Amir,^{4,†} Bobomurat Ahmedov,^{1,2,3,‡} and Sushant G. Ghosh^{4,5,§}¹*Institute of Nuclear Physics, Ulughbek, Tashkent 100214, Uzbekistan*²*Ulugh Beg Astronomical Institute, Astronomicheskaya 33, Tashkent 100052, Uzbekistan*³*National University of Uzbekistan, Tashkent 100174, Uzbekistan*⁴*Centre for Theoretical Physics, Jamia Millia Islamia, New Delhi 110025, India*⁵*Astrophysics and Cosmology Research Unit, School of Mathematics, Statistics and Computer Science, University of KwaZulu-Natal, Private Bag X54001, Durban 4000, South Africa*

(Received 18 February 2016; published 3 May 2016)

We study the shadows cast by the different types of rotating regular black holes viz. Ayón-Beato-García (ABG), Hayward, and Bardeen. These black holes have in addition to the total mass (M) and rotation parameter (a), different parameters as electric charge (Q), deviation parameter (g), and magnetic charge (g_*). Interestingly, the size of the shadow is affected by these parameters in addition to the rotation parameter. We found that the radius of the shadow in each case decreases monotonically, and the distortion parameter increases when the values of these parameters increase. A comparison with the standard Kerr case is also investigated. We have also studied the influence of the plasma environment around regular black holes to discuss its shadow. The presence of the plasma affects the apparent size of the regular black hole's shadow to be increased due to two effects: (i) gravitational redshift of the photons and (ii) radial dependence of plasma density.

DOI: [10.1103/PhysRevD.93.104004](https://doi.org/10.1103/PhysRevD.93.104004)**I. INTRODUCTION**

As we know, black holes are not visible objects; hence, it is interesting to study the null geodesics around them. The photons can be considered to extract the information from the black holes. This occurs by gravitational lensing by the black holes, which has been demonstrated for the last few decades by several authors. Both the deflection of light and the change in apparent brightness of the radiating source by a gravitational field are known as gravitational lenses. In many cases the lensing in the weak gravitational field approximation describes the scenario fully. However, in the case of ultracompact hypothetical objects like boson stars, the occurrence of the light rings are due to strong gravitational lensing (see, e.g., [1]). Various authors have studied gravitational lenses with a rotating black hole as a deflector [2] and focused only on the null geodesics motion at the equatorial plane. For example, the gravitational lensing by the Kerr black hole is discussed in [3–8]. The apparent shape of the nonrotating black holes is a perfect circle, while it is deformed for the rotating black holes due to the presence of spin [9,10]. The topic of gravitational lensing has been discussed by several authors with the expectation that the direct observation of black hole horizons will be possible in the near future [11–13].

To resolve the invisibility of the black hole, there is the Event Horizon Telescope (EHT)¹ to achieve the angular resolution comparable to a black hole shadow. A black hole

casts a shadow if it is in front of a distant bright object. The investigation of observing the black hole shadow is very interesting and a useful tool for measuring the nature of astrophysical black holes. The observation of the shadow also provides a tentative way to find the parameters of the black hole.

The shadow cast by the Schwarzschild black hole is first discussed by Synge [14] and Lunin [15]. Synge gave a formula to calculate the angular radius of the shadow. Bardeen [9] was the first to study the appearance of the shadow cast by the Kerr black hole; the result can be seen in Chandrasekhar's book [10] and in [16]. It can be seen that for Kerr black hole the shadow is no longer circular. The shadow of the Kerr black hole or a Kerr naked singularity by constructing two observables has been discussed by Hioki and Maeda [17]. Recently, some authors of this paper have developed new coordinate-independent formalism to describe the shadow of the black holes [18]. This subject for other black holes has been discussed by several authors, e.g., the Kerr-Newman black hole [16,19], Einstein-Maxwell-Dilaton-Axion black hole [20], Kerr-Taub-NUT black hole [21], rotating braneworld black hole [22], Kaluza-Klein rotating dilaton black hole [23], rotating non-Kerr black hole [24], and Kerr-Newman-NUT black holes with a cosmological constant [25]. The subject of getting a shadow has also been extended for the 5D rotating Myers-Perry black hole [26]. An example of a single black hole solution of general relativity with multiple shadows has been shown, for the first time, in [1]. The constraining the black holes and other compact objects parameters are wide discussed in the Refs. [27].

Falcke *et al.* [28] have initiated that very long baseline interferometry radio interferometers with advanced high

*ahmadjon@astrin.uz

†amirctp12@gmail.com

‡ahmedov@astrin.uz

§sghosh2@jmi.ac.in

¹<http://www.eventhorizontelescope.org/>.

spatial resolution would be able to resolve the supermassive black hole event horizon located at the center of either the Milky Way or the M87 galaxy in the submillimeter wavelength diapason (see, for the further details, [29–31]).

In this paper our aim is to extend the discussion of the black hole shadow for rotating regular black holes (e.g., Ayón-Beato-García, Hayward, and Bardeen) and to see the effect of the parameters on the size of a shadow and on the distortion of a shadow. We also plan to study the influence of the plasma on the optical properties of regular black holes. Our recent paper has been devoted to studying the optical properties of the Kerr black hole [32]. We have recently studied the particle motion as well as Penrose process around rotating regular black holes [33]. The influence of plasma to the shadow of static black holes has been considered in [34]. Optical phenomena in the field of the braneworld Kerr black hole has been studied in [35]. The analyzation of the circular geodesics around some regular black holes have been presented in [36]. Optical and other properties of Kerr superspinars have been considered in [37–39]. Gravitational lensing effects have been widely studied in the literature [34,40–44].

The paper is organized as follows. In Sec. II, we study the apparent shape of the shadow of the rotating Ayón-Beato-García (ABG) black hole and calculate the corresponding observable. We discuss the energy emission rate of the ABG black hole in a subsection of Sec. II. In Sec. III, we study the apparent shape of the shadow cast by the rotating Hayward and Bardeen black holes and also see the behavior of the observable, and in the subsection we study the energy emission rate for the rotating Hayward and Bardeen black holes. Section IV is devoted to studying the plasma influence on the shadow of regular black holes. We conclude our results in Sec. V. We have fixed units such that $G = c = 1$.

II. ROTATING AYÓN-BEATO-GARCÍA BLACK HOLE

We start with the rotating Ayón-Beato-García (ABG) spacetime, which is a nonsingular exact black hole solution of Einstein field equations coupled to a nonlinear electrodynamics that satisfies the weak energy condition. This spacetime class was introduced by Ayón-Beato *et al.* [45–47], and the rotating one is discussed by Toshmatov *et al.* [48,49]. The background metric of a rotating ABG spacetime in the Boyer-Lindquist coordinates (t, r, θ, ϕ) reads

$$ds^2 = -f(r, \theta)dt^2 + \frac{\Sigma}{\Delta} dr^2 - 2a \sin^2 \theta (1 - f(r, \theta)) d\phi dt + \Sigma d\theta^2 + \sin^2 \theta [\Sigma - a^2 (f(r, \theta) - 2) \sin^2 \theta] d\phi^2, \quad (1)$$

where the metric function $f(r, \theta)$ is given by

$$f(r, \theta) = 1 - \frac{2Mr\sqrt{\Sigma}}{(\Sigma + Q^2)^{3/2}} + \frac{Q^2 \Sigma}{(\Sigma + Q^2)^2}, \quad (2)$$

with

$$\Delta = \Sigma f(r, \theta) + a^2 \sin^2 \theta, \quad \Sigma = r^2 + a^2 \cos^2 \theta, \quad (3)$$

where M is the mass, a is rotation parameter, and Q is the electric charge of the black hole. The stationary and axial-symmetric metric (1) contains four constants of motion, which are the Lagrangian (\mathcal{L}), energy (E), z -component of angular momentum (L_z), and Carter constant (\mathcal{K}).

In order to discuss the black hole shadow, we need to calculate the geodesic equations of the photons for the metric (1). It is very difficult to separate the constants when we apply the Hamilton-Jacobi formulation for the rotating ABG spacetime because the function $f(r, \theta)$ has a very complicated form. Therefore, to resolve this problem, we consider an approximation in θ , such that $\theta \approx \pi/2 + \epsilon$, where ϵ is small angle. Note that here we consider the near-equatorial plane orbits of the photons; however, unstable photon circular orbits are not restricted necessarily to the equatorial plane. This fact does not render the calculations below since in this paper our main aim is calculating the shadow of the black hole by the observer at infinity, which can indeed be obtained using the above-mentioned approximation. Furthermore, as the observer is situated far away from the black hole, the photons will arrive near the equatorial plane (see for details Sec. IIIA). In this case the trigonometric functions take the form of $\sin \theta = 1$ and $\cos \theta = \epsilon$, and the function $f(r)$ is given in simple form:

$$f(r) = 1 - \frac{2Mr^2}{(r^2 + Q^2)^{3/2}} + \frac{Q^2 r^2}{(r^2 + Q^2)^2}. \quad (4)$$

We can easily get the following geodesic equations by solving equations $E = -p_t = -\partial \mathcal{L} / \partial \dot{t}$ and $L_z = p_\phi = \partial \mathcal{L} / \partial \dot{\phi}$, simultaneously

$$r^2 \frac{dt}{d\sigma} = a(L_z - aE) + \frac{r^2 + a^2}{\Delta} [(r^2 + a^2)E - aL_z], \quad (5)$$

$$r^2 \frac{d\phi}{d\sigma} = (L_z - aE) + \frac{a}{\Delta} [(r^2 + a^2)E - aL_z] \quad (6)$$

where σ is an affine parameter along the geodesics. Now, we can easily find out the remaining geodesic equations by using the Hamilton-Jacobi formulation. The corresponding Hamilton-Jacobi equation has the following form:

$$\frac{\partial S}{\partial \sigma} = -\frac{1}{2} g^{\mu\nu} \frac{\partial S}{\partial x^\mu} \frac{\partial S}{\partial x^\nu}, \quad (7)$$

where S is Jacobi action. If we have a separable solution, then it takes the following form:

$$S = \frac{1}{2} m_0^2 \sigma - Et + L_z \phi + S_r(r) + S_\epsilon(\epsilon), \quad (8)$$

where $S_r(r)$ and $S_\epsilon(\epsilon)$ are functions of r and ϵ , respectively. Inserting Eq. (8) into Eq. (7) and separating out the coefficients of r and ϵ being equal to the Carter constant, then we can easily get the geodesic equations in the following form:

$$r^2 \frac{dr}{d\sigma} = \pm \sqrt{\mathcal{R}}, \quad (9)$$

$$r^2 \frac{d\epsilon}{d\sigma} = \pm \sqrt{\Theta}, \quad (10)$$

where

$$\mathcal{R} = [(r^2 + a^2)E - aL_z]^2 - \Delta[\mathcal{K} + (L_z - aE)^2], \quad (11)$$

$$\Theta = \mathcal{K}, \quad (12)$$

where “+” and “−” signs in Eq. (9) correspond to the outgoing and ingoing photons in radial direction and in Eq. (10) correspond to the photons moving to the north ($\theta = 0$) and south ($\theta = \pi$) poles, respectively. The above geodesic equations indicate the propagation of light in the rotating ABG spacetime. To determine the unstable circular orbits, we introduce $\xi = L_z/E$ and $\eta = \mathcal{K}/E^2$. The condition for the unstable circular orbits is given by $\mathcal{R}(r) = 0$ and $d\mathcal{R}(r)/dr = 0$. Hence, from Eq. (11),

$$(r^2 + a^2 - a\xi)^2 - [\eta + (\xi - a)^2](r^2 f(r) + a^2) = 0, \quad (13)$$

$$\begin{aligned} & - [\eta + (\xi - a)^2](2rf(r) + r^2 f'(r)) \\ & + 4r(r^2 + a^2 - a\xi) = 0. \end{aligned} \quad (14)$$

Now we can easily obtain the expressions for the parameters ξ and η from Eqs. (13) and (14). These parameters take the following simple form:

$$\xi = \frac{(r^2 + a^2)(rf'(r) + 2f(r)) - 4(r^2 f(r) + a^2)}{a(rf'(r) + 2f(r))}, \quad (15)$$

$$\eta = \frac{r^3[8a^2 f'(r) - r(rf'(r) - 2f(r))^2]}{a^2(rf'(r) + 2f(r))^2}, \quad (16)$$

where r is the radius of the unstable circular orbits and

$$\begin{aligned} f'(r) = & -\frac{4Q^2 r^3}{(Q^2 + r^2)^3} + \frac{6Mr^3}{(Q^2 + r^2)^{5/2}} + \frac{2Q^2 r}{(Q^2 + r^2)^2} \\ & - \frac{4Mr}{(Q^2 + r^2)^{3/2}}. \end{aligned} \quad (17)$$

These two equations determine the contour of the shadow in the (ξ, η) plane. Furthermore, the parameters ξ and η satisfy the following relation:

$$\begin{aligned} \xi^2 + \eta = & 2r_0^2 + a^2 + \frac{16(r_0^2 f(r_0) + a^2)}{(r_0 f'(r_0) + 2f(r_0))^2} \\ & - \frac{8(r_0^2 f(r_0) + a^2)}{r_0 f'(r_0) + 2f(r_0)}. \end{aligned} \quad (18)$$

If we assume that $a = 0$ and $Q = 0$, then it corresponds to the Schwarzschild black hole, and the above relation reduces to

$$\xi^2 + \eta = \frac{2r_0^2(r_0^2 - 3)}{(r_0 - 1)^2}. \quad (19)$$

The shape of the critical curve for the Schwarzschild black hole is well known since for this case we have $r_0 = 3$; therefore, $\eta = 27 - \xi^2$.

A. Shadow of the rotating ABG black hole

Now we plan to determine the apparent shape of the rotating ABG black hole shadow. We consider celestial coordinates α and β to find the location of the shadow for a better visualization. The coordinate α corresponds to the apparent perpendicular distance of the shape as seen from the axis of symmetry, and the coordinate β is the apparent perpendicular distance of the shape from its projection on the equatorial plane. The schematic illustration of the celestial coordinates is presented in Fig. 1. The apparent shape of the black hole shadow for an observer which is far away from the black hole can be given by the celestial coordinates α and β :

$$\alpha = \lim_{r_0 \rightarrow \infty} \left(-r_0^2 \sin \theta_0 \frac{d\phi}{dr} \right), \quad (20)$$

$$\beta = \lim_{r_0 \rightarrow \infty} \left(r_0^2 \frac{d\epsilon}{dr} \right), \quad (21)$$

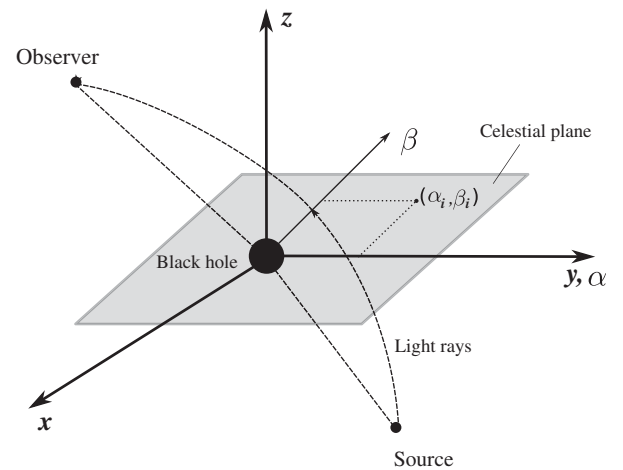


FIG. 1. Schematic illustration of the distant observer's celestial plane and celestial coordinates.

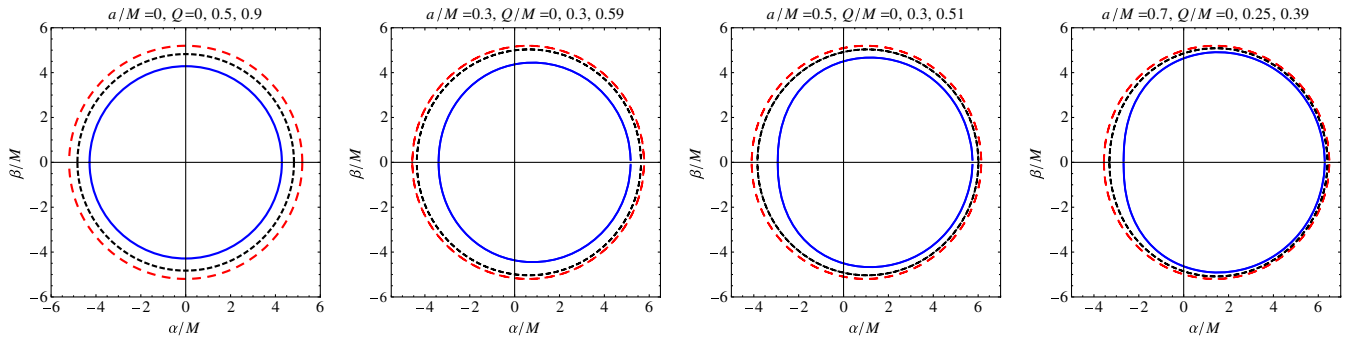


FIG. 2. Plot showing the silhouette of the shadow cast by the rotating ABG black hole for different values of parameters a/M and Q . The top left panel corresponds to the static black hole where the radius of the black hole decreases with an increase in parameter Q .

where according to the standard procedure r_0 is the distance from the black hole to the far observer; the celestial coordinates α and β are responsible for the apparent perpendicular distance between the bright image around the black hole due to the light rays falling into the event horizon and (i) the symmetry axis and (ii) its projection on the equatorial plane, respectively; θ_0 is the angle between the rotation axis of the black hole and the line of sight of the observer. Furthermore, we calculate $d\phi/dr$ and $d\epsilon/dr$ and substitute these values in the above expressions for the limit $r \rightarrow \infty$; then, we have

$$\alpha = -\xi, \quad (22)$$

and

$$\beta = \pm\sqrt{\eta}. \quad (23)$$

The silhouette of the shadow cast by the rotating ABG black hole can be visualized from Fig. 2. We can see from Fig. 2 that for a nonrotating case ($a/M = 0$), the silhouette of the shadow is a perfect circle, and the size of the

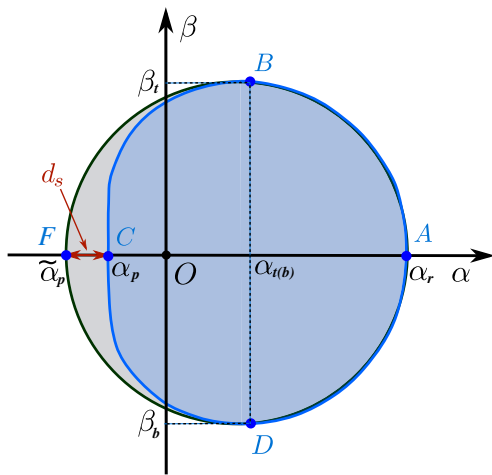


FIG. 3. Schematic representation of the black hole shadow and reference circle; d_s is the distance between the left point of the shadow and the reference circle.

silhouette decreases when the charge Q increases. Furthermore, in a rotating case ($a/M \neq 0$), the silhouette is a deformed circle which is more deformed if a/M takes an extremal value (cf. Fig. 2).

To analyze the shape of the shadow in detail, we define two astronomical observables: R_s , which describes the approximate size of the shadow, and δ_s , which measures its deformation. As suggested in Ref. [17] the circle of the shadow passing through the three points B (α_t, β_t) top one, D (α_b, β_b) bottom one, and A ($\alpha_r, 0$) most right one. The schematic representation of the above-mentioned definitions is shown in Fig 3. The radius or size of the shadow can be calculated through

$$R_s = \frac{(\alpha_t - \alpha_r)^2 + \beta_t^2}{2|\alpha_t - \alpha_r|}, \quad (24)$$

and the distortion parameter is given as

$$\delta_s = \frac{d_s}{R_s} = \frac{\tilde{\alpha}_p - \alpha_p}{R_s}, \quad (25)$$

where the points F ($\tilde{\alpha}_p, 0$) and C ($\alpha_p, 0$) cut the horizontal axis at the opposite side of ($\alpha_r, 0$), and d_s is the distance between the left point of the shadow and the reference circle (cf. Fig. 3). We can see the behavior of the observables R_s and δ_s as a function of charge Q in both nonrotating and rotating black hole cases from Fig. 4. It can be observed from Fig. 4 that the presence of charge Q affects the size of the shadow as well as the distortion parameter, i.e., the size of the shadow decreases and the distortion parameter increases with charge Q .

B. Energy emission rate of rotating ABG black hole

In the preceding subsection we have discussed possible visibility of a rotating regular black through its shadow, and we have mentioned in our previous study [26] that at high energy the cross section of the absorption of a black hole slightly modulates near a limiting constant value. Consequently, the shadow of the black hole is responsible for high energy absorption cross section by the black hole

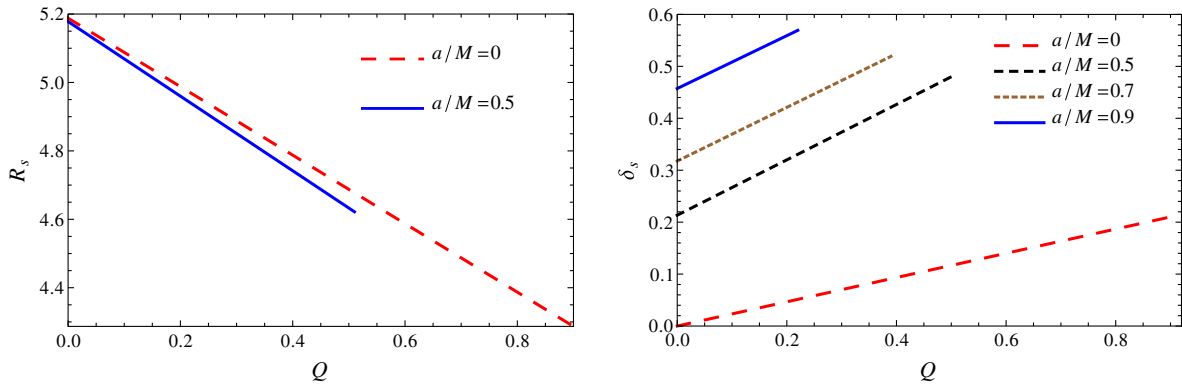


FIG. 4. Plots showing the behavior of R_s vs Q (left plot) and δ_s vs Q (right plot) of the rotating ABG black hole for the different values of a/M .

for the distant observer at infinity. The value of the mentioned limiting constant value is derived in terms of geodesics and can be analyzed for wave theories. For a black hole endowed with a photon sphere, the limiting constant value is the same as the geometrical cross section of this photon sphere [50]. Here, the limiting constant value of the absorption cross section for a spherically symmetric black hole can be given by [20]

$$\sigma_{\text{lim}} \approx \pi R_s^2, \quad (26)$$

and by using this limiting value, we can easily get the energy emission rate in the following form:

$$\frac{d^2 E(\omega)}{d\omega dt} = \frac{2\pi^2 R_s^2}{e^{\omega/T} - 1} \omega^3, \quad (27)$$

where ω represents the frequency of the photon, and the Hawking temperature (T) can be calculated as

$$T = -\frac{1}{4\pi r_+(a^2 + r_+^2)(Q^2 + r_+^2)^3} [2Q^6 r_+^2 + 3Q^4 r_+^4 + Q^2 r_+^6 - r_+^8 + a^2(Q^2 + r_+^2)^2(4Q^2 + r_+^2)], \quad (28)$$

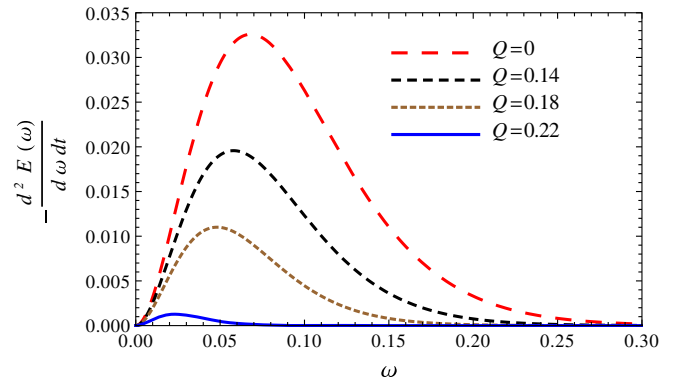
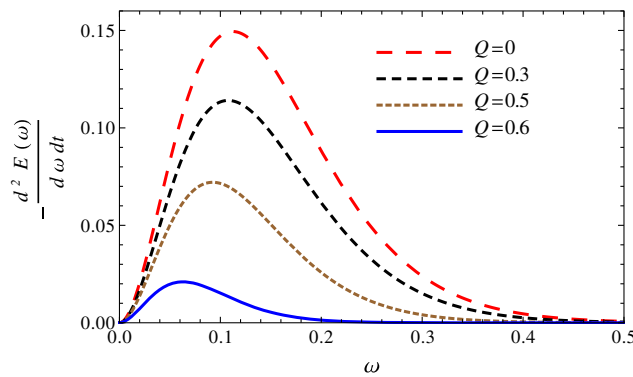


FIG. 5. Plot showing the behavior of energy emission rate vs the frequency (ω). (Left) For $a/M = 0$. (Right) For $a/M = 0.9$.

where r_+ is the outer event horizon of the rotating ABG black hole defined as the greater root of the solution for the condition g^{rr} . The plots of $d^2 E(\omega)/d\omega dt$ versus ω can be seen from Fig. 5 for $a/M = 0$ (left panel) and $a/M = 0.9$ (right panel).

III. ROTATING HAYWARD AND BARDEEN BLACK HOLES

The spacetime metric of the rotating Kerr-like black hole, in the Boyer-Lindquist coordinates [51], is given as

$$ds^2 = -\left(1 - \frac{2mr}{\Sigma}\right) dt^2 - \frac{4amr\sin^2\theta}{\Sigma} dt d\phi + \frac{\Sigma}{\Delta} dr^2 + \Sigma d\theta^2 + \left(r^2 + a^2 + \frac{2a^2mr\sin^2\theta}{\Sigma}\right) \sin^2\theta d\phi^2, \quad (29)$$

where

$$\Sigma = r^2 + a^2 \cos^2\theta, \quad \Delta = r^2 - 2mr + a^2. \quad (30)$$

The above metric represents Kerr black hole spacetime, if $m \rightarrow M$. In this case, mass m depends on r , which is given by

$$m \rightarrow m_h = M \frac{r^3}{r^3 + g^3}, \quad (31)$$

and

$$m \rightarrow m_b = M \left(\frac{r^2}{r^2 + g_*^2} \right)^{3/2}, \quad (32)$$

where black hole masses m_h and m_b correspond to the rotating Hayward and rotating Bardeen regular black holes, respectively. The constants a , g , and g_* correspond to the rotation parameter, deviation parameter, and magnetic charge due to the nonlinear electromagnetic field, respectively. The corresponding geodesic equations of these black holes have the same form, and the difference is just due to the different mass. One can easily find the equations in the following form:

$$\Sigma \frac{dt}{d\sigma} = a(L_z - aE \sin^2 \theta) + \frac{r^2 + a^2}{\Delta} [(r^2 + a^2)E - aL_z], \quad (33)$$

$$\Sigma \frac{d\phi}{d\sigma} = \left(\frac{L_z}{\sin^2 \theta} - aE \right) + \frac{a}{\Delta} [(r^2 + a^2)E - aL_z], \quad (34)$$

$$\Sigma \frac{dr}{d\sigma} = \pm \sqrt{\mathcal{R}}, \quad (35)$$

$$\Sigma \frac{d\theta}{d\sigma} = \pm \sqrt{\Theta}, \quad (36)$$

where σ is an affine parameter, and

$$\mathcal{R} = [(r^2 + a^2)E - aL_z]^2 - \Delta[\mathcal{K} + (L_z - aE)^2], \quad (37)$$

$$\Theta = \mathcal{K} + \cos^2 \theta \left(a^2 E^2 - \frac{L_z^2}{\sin^2 \theta} \right). \quad (38)$$

Note that in this section the equations of motion are not restricted to be at the equatorial plane ($\theta \neq \text{const}$). With the

help of the condition for the unstable circular orbits of the particles, i.e., $\mathcal{R}(r) = 0$ and $d\mathcal{R}(r)/dr = 0$, we have

$$r^4 + (a^2 - \xi^2 - \eta)r^2 + 2m[\eta + (\xi - a)^2]r - a^2\eta = 0, \quad (39)$$

$$4r^3 + 2(a^2 - \xi^2 - \eta)r + 2m[\eta + (\xi - a)^2] - 2m'[\eta + (\xi - a)^2]r = 0. \quad (40)$$

By solving the above equations simultaneously, we can easily get the parameters ξ and η as

$$\xi = \frac{m(a^2 - 3r^2) + r(r^2 + a^2)(m' + 1)}{a[m + r(m' - 1)]}, \quad (41)$$

$$\eta = -\frac{r^3}{a^2} [(1 + m'^2)r^3 + 2m'(r^2 - 3mr + 2a^2)r - m(6r^2 - 9mr + 4a^2)][m + r(m' - 1)]^{-2}, \quad (42)$$

where m' represents the derivative of m with respect to r .

A. Shadow of rotating Hayward and Bardeen black holes

Now we calculate the celestial coordinates for these black holes which take the following form:

$$\alpha = -\xi \csc \theta_0, \quad (43)$$

$$\beta = \pm \sqrt{\eta + a^2 \cos^2 \theta_0 - \xi^2 \cot^2 \theta_0}, \quad (44)$$

where θ_0 is the angle between the rotation axis of the black hole and the line of sight of the distant observer. Note that these expressions are valid for a far away observer by the definition [see Eqs. (20) and (21)]. If we set the inclination angle to equatorial plane $\theta_0 = \pi/2$, then the celestial coordinates have the following simple form:

$$\alpha = -\xi, \quad (45)$$

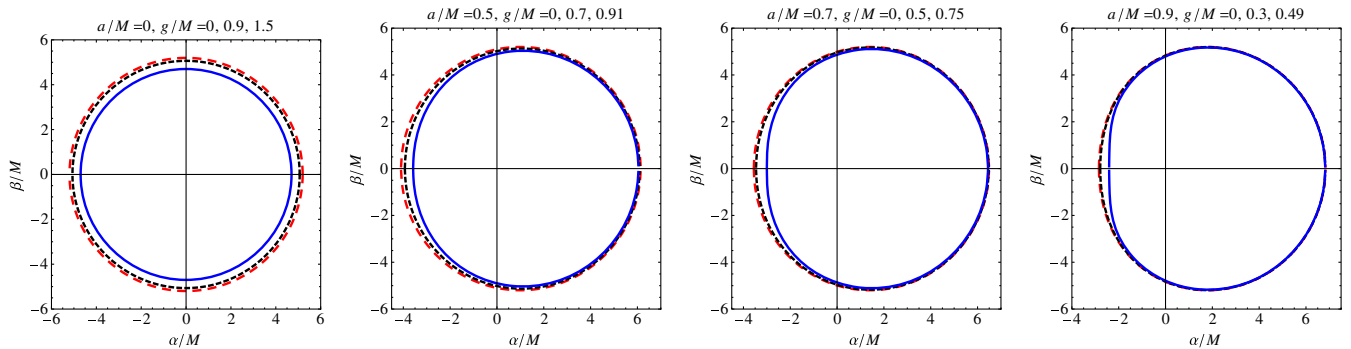


FIG. 6. Plot showing the silhouette of the shadow cast by the rotating Hayward black hole for the different values of the rotation parameter a/M . In all plots the outer red lines correspond to $g/M = 0$.

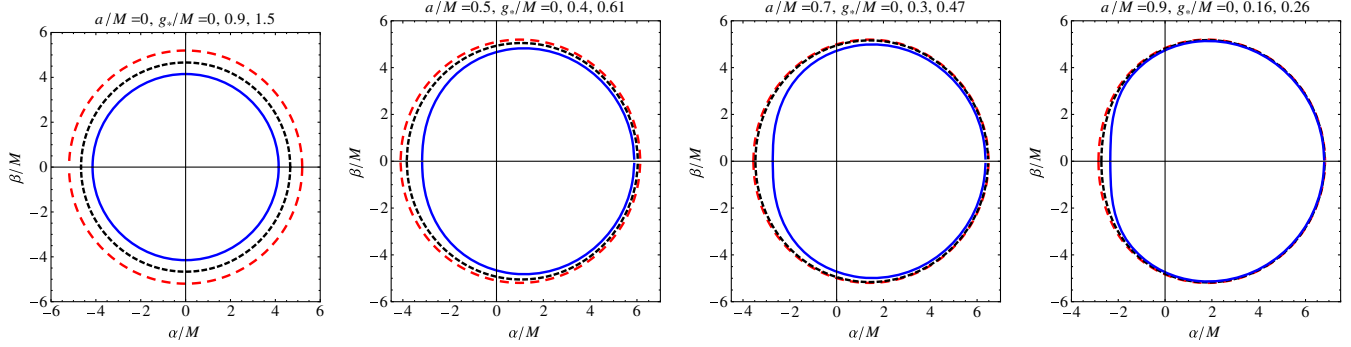


FIG. 7. Plot showing the silhouette of the shadow cast by the Bardeen black hole for the different values of the rotation parameter a/M . In all plots the outer red lines correspond to $g_*/M = 0$.

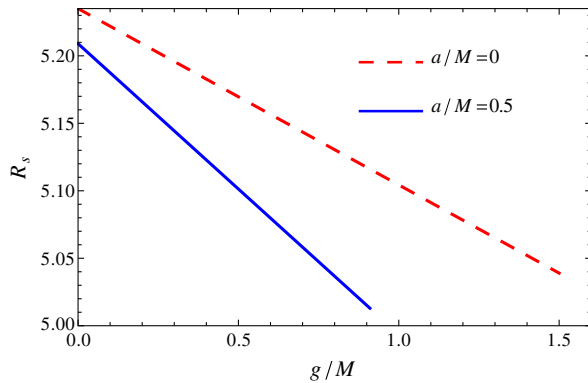
$$\beta = \pm\sqrt{\eta}. \quad (46)$$

To visualize the shadow cast by the rotating Hayward and Bardeen black holes, we need to make some plots for the coordinates α/M and β/M . These plots can be seen from Figs. 6 and 7 for the fixed values of spin parameter a/M and different values of parameters g/M and g_*/M . We can easily observe the effect of parameters g/M and g_*/M on the silhouette of a shadow: an increase in the value of g/M and g_*/M decreases the size of the silhouette of the shadow. The silhouette of the shadow is more deformed for the extremal value of a/M (c.f. Figs. 6 and 7).

The behavior of the observable R_s and δ_s introduced in Sec. II can be seen from Figs. 8 and 9. In both black hole cases, we observe that the radius of the silhouette of the shadow decreases and the distortion parameter increases monotonically.

B. Energy emission rate

Now we discuss the energy emission rate for both rotating Hayward and Bardeen black holes. It has the following form [20]:



$$\frac{d^2 E(\omega)}{d\omega dt} = \frac{2\pi^2 R_s^2}{e^{\omega/T} - 1} \omega^3, \quad (47)$$

where for the rotating Hayward black hole, the Hawking temperature reads

$$T_h = \frac{1}{4\pi(r_+^2 + a^2)(r_+^3 + g^3)} [2r_+^2(r_+^3 + g^3) - 4r_+(r_+^2 + a^2)(r_+^3 + g^3) + 3r_+^2(r_+^2 + a^2)], \quad (48)$$

and for rotating Bardeen black hole, it has the following form:

$$T_b = -\frac{1}{4\pi r_+(r_+^2 + a^2)(r_+^2 + g_*^2)} [4(r_+^2 + a^2)(r_+^2 + g_*^2) + 2r_+^2(r_+^2 + g_*^2) + 3r_+^2(r_+^2 + a^2)]. \quad (49)$$

Next, to see the behavior of the energy emission rate, we plot $d^2 E(\omega)/d\omega dt$ versus ω for both of the black holes. It can be seen from Fig. 10 that the representation is made for spin $a/M = 0.9$ and different values of parameters g/M and g_*/M .

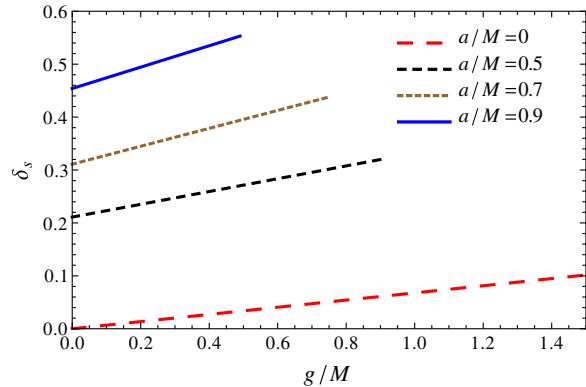
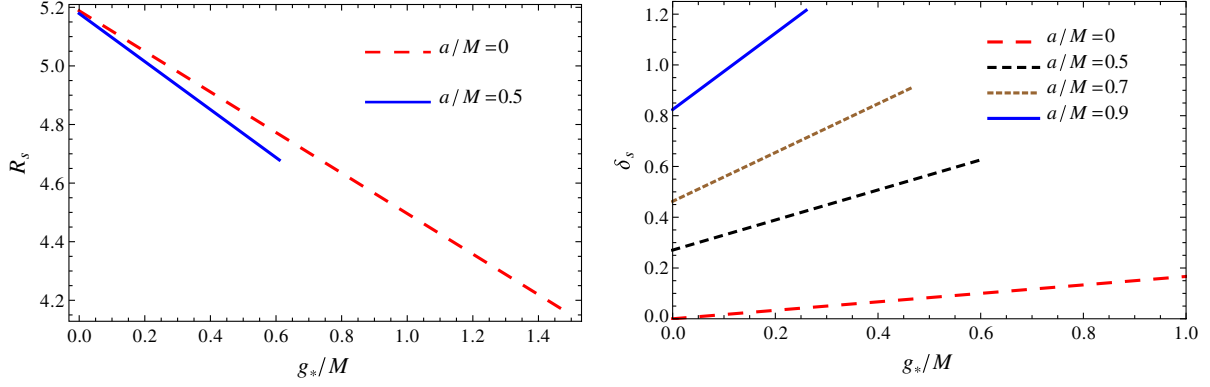


FIG. 8. Plots showing the behavior of R_s vs g/M (left panel) and δ_s vs g/M (right panel) of the rotating Hayward black hole for the different values of the rotation parameter a/M .


 FIG. 9. Plots showing the behavior of R_s vs g_*/M (left panel) and δ_s vs g_*/M (right panel) of the rotating Bardeen black hole.

IV. SHADOW OF REGULAR BLACK HOLE IN THE PRESENCE OF PLASMA

Now we consider the shadow of the regular black hole in the presence of the plasma. We use the model of the plasma with the refraction index to be equal to $n = n(x^i, \omega)$, where ω is the photon frequency measured by an observer with velocity u^α . The so-called effective energy of a photon has the form $\hbar\omega = -p_\alpha u^\alpha$. In Ref. [52] the expression for the refraction index of the plasma has been obtained in the form:

$$n^2 = 1 + \frac{P_\alpha P^\alpha}{(p_\beta u^\beta)^2}. \quad (50)$$

Note that in the case of absence of the plasma one has the value for the refraction index $n = 1$. Using the Hamiltonian for the photon in the form

$$H(x^\alpha, p_\alpha) = \frac{1}{2} [g^{\alpha\beta} p_\alpha p_\beta + (n^2 - 1)(p_\beta u^\beta)^2] = 0 \quad (51)$$

one can obtain the equations of motion for the photons around regular black holes in the presence of the plasma. We introduce the two frequencies of electromagnetic waves; the first one is associated with a timelike Killing

vector ξ^α , i.e., $\omega_\xi = -k^\alpha \xi_\alpha$, and other one is measured by an observer having a four-velocity u^α , i.e., $\omega = -k^\alpha u_\alpha$, where k^α is a null wave vector [32].

Hereafter, we use the specific form for the plasma frequency in the form

$$n^2 = 1 - \frac{\omega_e^2}{\omega^2}, \quad (52)$$

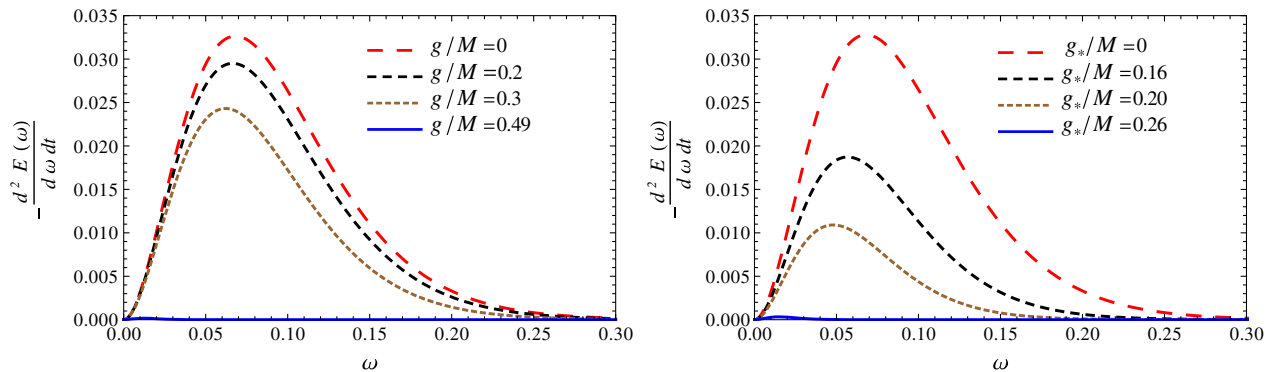
where ω_e is usually called plasma frequency.

Using the Hamilton-Jacobi method described in Sec. II, one may easily obtain the equations of motion for the photons around the Hayward and Bardeen regular black holes in the presence of plasma as

$$\Sigma \frac{dt}{d\sigma} = a(L_z - n^2 E a \sin^2 \theta) + \frac{r^2 + a^2}{\Delta} [(r^2 + a^2) n^2 E - a L_z], \quad (53)$$

$$\Sigma \frac{d\phi}{d\sigma} = \left(\frac{L_z}{\sin^2 \theta} - a E \right) + \frac{a}{\Delta} [(r^2 + a^2) E - a L_z], \quad (54)$$

$$\Sigma \frac{dr}{d\sigma} = \pm \sqrt{\mathcal{R}_p}, \quad (55)$$


 FIG. 10. Plot showing the behavior of energy emission rate vs the frequency (ω) for $a/M = 0.9$. (Left) For Hayward. (Right) For Bardeen.

$$\Sigma \frac{d\theta}{d\sigma} = \pm \sqrt{\Theta_p}, \quad (56)$$

where the functions $\mathcal{R}_p(r)$ and $\Theta_p(\theta)$ are introduced as

$$\mathcal{R}_p = [(r^2 + a^2)E - aL_z]^2 + (r^2 + a^2)^2(n^2 - 1)E^2 - \Delta[\mathcal{K} + (L_z - aE)^2], \quad (57)$$

$$\Theta_p = \mathcal{K} + \cos^2\theta \left(a^2 E^2 - \frac{L_z^2}{\sin^2\theta} \right) - (n^2 - 1)a^2 E^2 \sin^2\theta. \quad (58)$$

For the plasma frequency ω_e , we use the expression

$$\omega_e^2 = \frac{4\pi e^2 N(r)}{m_e}, \quad (59)$$

where e and m_e are the electron charge and mass, respectively, and $N(r)$ is the plasma number density. We consider a radial power-law density [44]

$$N(r) = \frac{N_0}{r^h}, \quad (60)$$

where $h \geq 0$, such that

$$\omega_e^2 = \frac{k}{r^h}. \quad (61)$$

As an example here we get the value for power h as 1 [44].

The shadow of the black hole in the plasma environment can be found using the conditions as was done in the previous sections:

$$\mathcal{R}(r) = 0 = \partial\mathcal{R}(r)/\partial r.$$

Using these equations one can easily find the expressions for the parameters ξ and η in the form

$$\xi = \frac{\mathcal{B}}{\mathcal{A}} + \sqrt{\frac{\mathcal{B}^2}{\mathcal{A}^2} - \frac{\mathcal{C}}{\mathcal{A}}}, \quad (62)$$

$$\eta = \frac{(r^2 + a^2 - a\xi)^2 + (r^2 + a^2)^2(n^2 - 1)}{\Delta} - (\xi - a)^2, \quad (63)$$

where we have used the following notations

$$\mathcal{A} = \frac{a^2}{\Delta}, \quad (64)$$

$$\mathcal{B} = \frac{a m a^2 - m r^2 + r^3 m' + a^2 r m'}{\Delta m - r + r m'}, \quad (65)$$

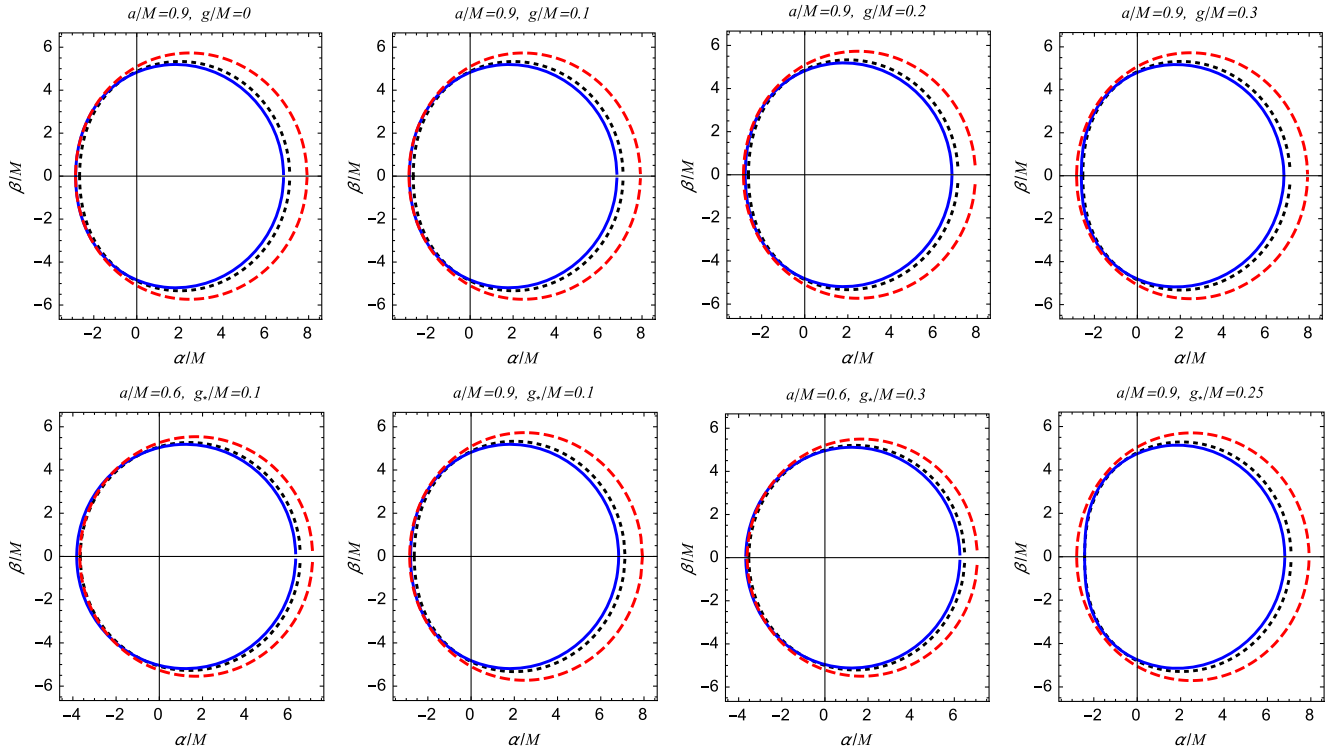


FIG. 11. Plot showing the silhouette of the shadow cast by the Hayward and Bardeen regular black holes surrounded by plasma for the different values of the rotation parameter a/M and the refraction index. The solid lines in the plots correspond to the vacuum case, while for the dotted and dashed lines we choose the plasma frequency $\omega_e/\omega_\xi = k/r$, where $(k/M)^2 = 0.5$ and $(k/M)^2 = 1.0$, respectively. The inclination angle between the observer and the axis of rotation has been taken to be $\theta_0 = \pi/2$.

$$C = n^2 \frac{(r^2 + a^2)^2}{\Delta} + \frac{2r(r^2 + a^2)n^2 - (r^2 + a^2)^2 nn'}{m - r + rm'}, \quad (66)$$

and the prime denotes the differentiation with respect to radial coordinate r . The functions Δ and m are defined as in Eqs. (30)–(32).

The expression for the celestial coordinates take the following form:

$$\alpha = -\frac{\xi}{n \sin \theta}, \quad (67)$$

$$\beta = \frac{\sqrt{\eta + a^2 - n^2 a^2 \sin^2 \theta - \xi^2 \cot^2 \theta}}{n}, \quad (68)$$

for the case when the black hole is surrounded by plasma.

In Fig. 11 the silhouettes of the shadow of the rotating Hayward and Bardeen black holes for different values of the black hole rotation parameter a/M and parameters g/M and g_*/M are presented. In these figures we choose the plasma frequency in the form $\omega_e/\omega_\xi = k/r$. From Fig. 11 one can easily see that the presence of the plasma affects the apparent size of the shadow to be increased, while we have shown that the parameters of the regular black holes force to decrease the shadow size. There is also a tendency to decrease the distortion of the shadow in the presence of plasma. Physically, this is similar to an effect of gravitational redshift of the photons in the gravitational field of the regular black holes: the frequency change due to the gravitational redshift affects the plasma refraction index.

V. CONCLUSION

In this paper, we have analyzed the shape of the shadow cast by different types of regular black holes. We have discussed how the shadow cast by these black holes is distorted by the presence of the various parameters related to regular black holes and the environment. In first part of the paper, we have studied the shadow cast by the rotating ABG black hole. We have found that the presence of the electric charge affected the shape of the shadow. We see that with increasing the value of a/M the shape of the shadow becomes more and more asymmetric with respect to the vertical axis. It can be seen that for the fixed value of spin the size of the shadow monotonically decreases as the electric charge increases. Furthermore, we calculate the deformation due to an increase in the spin of the black hole, which is characterized by the deformation parameter (δ_s). One can see that δ_s increases with an increase in the electric

charge as well as spin. Next, we have discussed the energy emission rate of the rotating ABG black hole. The energy emission rate decreases with an increase in the value of Q as well as in a/M . It can be seen from Fig. 5 that the peak is sharp for small values of Q .

In the next part of the paper, we have studied the shadow of the rotating Hayward and Bardeen black holes. The rotating Hayward black hole contains g/M , which provides deviation from the Kerr black hole, and the rotating Bardeen black hole has another parameter g_*/M , which is a magnetic charge due to the nonlinear electromagnetic field. Furthermore, we see the effect of the parameters g/M and g_*/M on the shape of the black hole shadow. We have found that the presence of the parameters g/M and g_*/M decreases the size of the silhouette of the shadow for each fixed value of a/M . There is an increase in δ_s when a is increasing, and we get an extremal value for both black holes. One can also see the behavior of the energy emission rate versus frequency, which indicates that the energy emission rate decreases with increasing values of g/M and g_*/M .

In the last part of the paper, we have also studied the influence of the plasma environment around the Hayward and Bardeen regular black holes to the change of the size and shape of the regular black hole's shadow. It was shown that the presence of the plasma affects the apparent size of the shadow to be increased, while we observe the opposite effect for the magnetic charges of the regular black holes. There is also a tendency to decrease the distortion of the shadow in the presence of plasma. Physically, this is similar to an effect of gravitational redshift of the photons in the gravitational field of the regular black holes: the frequency change due to the gravitational redshift affects the plasma refraction index.

ACKNOWLEDGMENTS

M. A. acknowledges the University Grant Commission, India, for financial support through the Maulana Azad National Fellowship For Minority Students scheme (Grant No. F1-17.1/2012-13/MANF-2012-13-MUS-RAJ-8679) and the Institute of Nuclear Physics, Uzbekistan Academy of Sciences, for the great hospitality where this work was done. The research is supported in part by Projects No. F2-FA-F113, No. EF2-FA-0-12477, and No. F2-FA-F029 of the UzAS, by the ICTP through Grants No. OEA-PRJ-29 and No. OEA-NET-76, and by the Volkswagen Stiftung, Grant No. 86866. S. G. G. would like to thank SERB-DST for the Research Project Grant No. SB/S2/HEP-008/2014.

- [1] P. V. P. Cunha, C. A. R. Herdeiro, E. Radu, and H. F. Rúnarsson, *Phys. Rev. Lett.* **115**, 211102 (2015).
- [2] M. Sereno, *Mon. Not. R. Astron. Soc.* **344**, 942 (2003).
- [3] V. Bozza, *Phys. Rev. D* **67**, 103006 (2003).
- [4] S. E. Vázquez and E. P. Esteban, *Nuovo Cimento B* **119**, 489 (2004).
- [5] V. Bozza, F. de Luca, G. Scarpetta, and M. Sereno, *Phys. Rev. D* **72**, 083003 (2005).
- [6] V. Bozza, F. de Luca, and G. Scarpetta, *Phys. Rev. D* **74**, 063001 (2006).
- [7] V. Bozza and G. Scarpetta, *Phys. Rev. D* **76**, 083008 (2007).
- [8] G. V. Kraniotis, *Classical Quantum Gravity* **28**, 085021 (2011).
- [9] J. M. Bardeen, in *Black Holes (Les Astres Occlus)*, edited by C. Dewitt and B. S. Dewitt (Gordon and Breach, 1973), pp. 215–239.
- [10] S. Chandrasekhar, *The Mathematical Theory of Black Holes* (Oxford University Press, New York, 1998).
- [11] A. F. Zakharov, A. A. Nucita, F. De Paolis, and G. Ingrosso, *New Astron.* **10**, 479 (2005).
- [12] C.-K. Chan, D. Psaltis, F. Özel, R. Narayan, and A. Sądowski, *Astrophys. J.* **799**, 1 (2015).
- [13] D. Psaltis, R. Narayan, V. L. Fish, A. E. Broderick, A. Loeb, and S. S. Doeleman, *Astrophys. J.* **798**, 15 (2015).
- [14] J. L. Synge, *Mon. Not. R. Astron. Soc.* **131**, 463 (1966).
- [15] J.-P. Luminet, *Astron. Astrophys.* **75**, 228 (1979).
- [16] A. de Vries, *Classical Quantum Gravity* **17**, 123 (2000).
- [17] K. Hioki and K.-I. Maeda, *Phys. Rev. D* **80**, 024042 (2009).
- [18] A. A. Abdujabbarov, L. Rezzolla, and B. J. Ahmedov, *Mon. Not. R. Astron. Soc.* **454**, 2423 (2015).
- [19] R. Takahashi, *Publ. Astron. Soc. Jpn.* **57**, 273 (2005).
- [20] S.-W. Wei and Y.-X. Liu, *J. Cosmol. Astropart. Phys.* **11** (2013) 063.
- [21] A. Abdujabbarov, F. Atamurotov, Y. Kucukakca, B. Ahmedov, and U. Camci, *Astrophys. Space Sci.* **344**, 429 (2013).
- [22] L. Amarilla and E. F. Eiroa, *Phys. Rev. D* **85**, 064019 (2012).
- [23] L. Amarilla and E. F. Eiroa, *Phys. Rev. D* **87**, 044057 (2013).
- [24] F. Atamurotov, A. Abdujabbarov, and B. Ahmedov, *Phys. Rev. D* **88**, 064004 (2013).
- [25] A. Grenzebach, V. Perlick, and C. Lämmerzahl, *Phys. Rev. D* **89**, 124004 (2014).
- [26] U. Papnoi, F. Atamurotov, S. G. Ghosh, and B. Ahmedov, *Phys. Rev. D* **90**, 024073 (2014).
- [27] C. Bambi and K. Freese, *Phys. Rev. D* **79**, 043002 (2009). C. Bambi and N. Yoshida, *Classical Quantum Gravity* **27**, 205006 (2010). C. Bambi, F. Caravelli, and L. Modesto, *Phys. Lett. B* **711**, 10 (2012). C. Bambi, *Phys. Rev. D* **87**, 107501 (2013). Z. Li and C. Bambi, *J. Cosmol. Astropart. Phys.* **01** (2014) 041. N. Tsukamoto, Z. Li, and C. Bambi, *J. Cosmol. Astropart. Phys.* **06** (2014) 043.
- [28] H. Falcke, F. Melia, and E. Agol, *Astrophys. J. Lett.* **528**, L13 (2000).
- [29] R. Takahashi, *J. Korean Phys. Soc.* **45**, S1808 (2004); *Astrophys. J.* **611**, 996 (2004).
- [30] T. Johannsen and D. Psaltis, *Astrophys. J.* **716**, 187 (2010).
- [31] H. Falcke and S. B. Markoff, *Classical Quantum Gravity* **30**, 244003 (2013).
- [32] F. Atamurotov, B. Ahmedov, and A. Abdujabbarov, *Phys. Rev. D* **92**, 084005 (2015).
- [33] B. Toshmatov, A. Abdujabbarov, B. Ahmedov, and Z. Stuchlík, *Astrophys. Space Sci.* **357**, 41 (2015).
- [34] V. Perlick, O. Y. Tsupko, and G. S. Bisnovaty-Kogan, *Phys. Rev. D* **92**, 104031 (2015).
- [35] J. Schee and Z. Stuchlík, *Int. J. Mod. Phys. D* **18**, 983 (2009).
- [36] Z. Stuchlík and J. Schee, *Int. J. Mod. Phys. D* **24**, 1550020 (2015).
- [37] Z. Stuchlík and J. Schee, *Classical Quantum Gravity* **27**, 215017 (2010).
- [38] Z. Stuchlík and J. Schee, *Classical Quantum Gravity* **29**, 065002 (2012).
- [39] Z. Stuchlík and J. Schee, *Classical Quantum Gravity* **29**, 025008 (2012).
- [40] G. S. Bisnovaty-Kogan and O. Y. Tsupko, *Mon. Not. R. Astron. Soc.* **404**, 1790 (2010).
- [41] O. Y. Tsupko and G. S. Bisnovaty-Kogan, *Gravitation Cosmol.* **18**, 117 (2012).
- [42] V. S. Morozova, B. J. Ahmedov, and A. A. Tursunov, *Astrophys. Space Sci.* **346**, 513 (2013).
- [43] X. Er and S. Mao, *Mon. Not. R. Astron. Soc.* **437**, 2180 (2014).
- [44] A. Rogers, *Mon. Not. R. Astron. Soc.* **451**, 17 (2015).
- [45] E. Ayón-Beato and A. García, *Phys. Rev. Lett.* **80**, 5056 (1998).
- [46] E. Ayon-Beato, *Phys. Lett. B* **464**, 25 (1999).
- [47] E. Ayon-Beato and A. Garcia, *Gen. Relativ. Gravit.* **31**, 629 (1999).
- [48] B. Toshmatov, B. Ahmedov, A. Abdujabbarov, and Z. Stuchlík, *Phys. Rev. D* **89**, 104017 (2014).
- [49] M. Azreg-Aïnou, *Phys. Rev. D* **90**, 064041 (2014).
- [50] C. W. Misner, K. S. Thorne, and J. A. Wheeler, *Gravitation* (W. H. Freeman, San Francisco, 1973).
- [51] C. Bambi and L. Modesto, *Phys. Lett. B* **721**, 329 (2013).
- [52] J. L. Synge, *Relativity: The General Theory* (North-Holland, Amsterdam, 1960).